

# Molecular-Crowding-Induced Clustering of DNA-Wrapped Carbon Nanotubes for Facile Length Fractionation

Constantine Y. Khripin, Nicholas Arnold-Medabalimi, and Ming Zheng\*

Polymers Division, National Institute of Standards in Technology, 100 Bureau Drive, Gaithersburg, Maryland 20899-8542, United States

Much work has been dedicated to developing methods for fractionating single-wall carbon nanotubes (SWCNTs) based on their “chirality”, or molecular structure,<sup>1–3</sup> culminating in the recent isolation of nanotubes of nearly uniform chirality.<sup>4–9</sup> However, many emerging applications and fundamental studies require SWCNTs that are sorted by length. Long nanotubes are preferable for electronics applications;<sup>10</sup> they are also brighter fluorescently<sup>11–13</sup> which may be an important consideration for *in vivo* bioimaging applications.<sup>14</sup> On the other hand, short SWCNTs have been shown to preferentially enter mammalian cells.<sup>15</sup> Thus, length could be a factor for drug<sup>16,17</sup> and gene<sup>18,19</sup> delivery applications. SWCNT length may also play a role in the biodistribution of nanotubes used for *in vivo* imaging.<sup>19</sup> Yet in the majority of reported investigations, the nanotube raw material is not length fractionated.<sup>10,14,16</sup>

To date, several methods for SWCNT length fractionation have been demonstrated. Fractionation using size exclusion chromatography (SEC) has been explored.<sup>20–24</sup> Narrow size distributions (~10% standard deviation in length) have been achieved for small quantities,<sup>23</sup> however, this method requires a liquid chromatography apparatus. Ultracentrifugation methods have advantages in preparation scale, but resolution is less than that of SEC,<sup>25,26</sup> and expensive centrifuges are necessary. Other reported methods include field-flow fractionation<sup>27,28</sup> and cross-flow filtration.<sup>29</sup> Length-sorted SWCNTs obtained *via* these methods have enabled measurements of some length-dependent properties, such as cell membrane penetration,<sup>15</sup> Raman scattering<sup>30</sup> and photoluminescence.<sup>11,26</sup> Nevertheless, the use of length-sorted SWCNTs is not widespread, in part

**ABSTRACT** Emerging applications require single-wall carbon nanotubes (SWCNTs) of well-defined length. Yet the use of length-defined SWCNTs is limited, in part due to the lack of an easily accessible materials preparation method. Here, we present a new strategy for SWCNT length fractionation based on molecular crowding induced cluster formation. We show that the addition of polyethylene glycol (PEG) as a crowding agent into DNA-wrapped SWCNT dispersion leads to the formation of reversible, nematic, and rodlike microclusters, which can be collected by gentle centrifugation. Since shorter SWCNTs form clusters at higher polyethylene glycol concentration, gradual increase in PEG concentration results in length fractionated SWCNTs. Using atomic force microscopy (AFM) we show that fractions with average lengths of 60–500 nm and standard deviations of 30–40% can be obtained. The concept of molecular-crowding-based fractionation should be applicable to other nanoparticle dispersions.

**KEYWORDS:** carbon nanotube · DNA · molecular crowding · depletion forces · self-assembly

due to the expensive equipment required for techniques such as SEC and ultracentrifugation.

Here, we report a new fractionation technique, based on molecular-crowding-induced self-assembly of colloidal SWCNTs. The term “molecular crowding” comes from cell biology: intracellular environments can have as much as 40% inert components by volume,<sup>31</sup> which affect cellular processes such as DNA packing<sup>32</sup> and protein assembly.<sup>33</sup> Generally, the term can describe any environment with a high concentration of inert macromolecules. Under crowded conditions, entropic effects result in short-range attractive “depletion forces” between colloidal particles.<sup>34,35</sup> Consequently, the particles may form clusters in a process that has been variously described as self-assembly,<sup>36,37</sup> or phase separation.<sup>38,39</sup> Regardless of which theoretical description one uses, factors such as size and zeta potential<sup>40</sup> of the colloids affect their clustering in a crowded environment. Thus, selective precipitation can be achieved by carefully controlling crowding

\* Address correspondence to ming.zheng@nist.gov.

Received for review August 3, 2011 and accepted September 6, 2011.

Published online  
10.1021/nn2029549

© XXXX American Chemical Society

conditions.<sup>40,41</sup> This method has been applied to protein extraction and purification<sup>40</sup> as well as for length fractionation of double-stranded DNA.<sup>41</sup> To our knowledge, this method has not been used for the purification of nanoparticles.

DNA-wrapped SWCNTs are highly stable colloids in aqueous phase.<sup>42,43</sup> They have similar diameter and zeta potential to double-stranded DNA.<sup>44</sup> To understand how a crowded environment might produce length-dependent DNA–SWCNT cluster formation, we elaborate the entropic argument as follows.<sup>45</sup> In the presence of a crowding agent (such as polyethylene glycol (PEG), approximated as a sphere of diameter  $d$ ), a DNA–SWCNT (of diameter  $D$  and length  $L$ ) excludes a volume  $V_{\text{ex}} = 1/4 L \pi (d + D)^2$  from PEG centers of mass. When two DNA–SWCNTs approach and align, their excluded volumes overlap, increasing the free volume available to PEG and contributing to the overall reduction of the system's free energy. This results in an effective attractive, aligning force between DNA–SWCNT, which balances the repulsive electrostatic force, and leads to the clustering of DNA–SWCNT when PEG concentration is high enough (Figure 1A). Since the excluded volume is proportional to length, longer DNA–SWCNTs are expected to assemble at lower concentrations of PEG than shorter DNA–SWCNTs, which could be exploited to achieve length fractionation by selective precipitation.

In what follows, we first demonstrate that DNA–SWCNTs assemble into rodlike microclusters in the presence of PEG. Using polarized fluorescence microscopy we show that the DNA–SWCNTs align along the cluster axis; excitonic energy transfer (EET) measurements indicate that clustering is reversible. Tests on DNA–SWCNT samples length-fractionated by SEC reveal that longer nanotubes form clusters at lower PEG concentrations. On the basis of these observations, we present two selective precipitation schemes: a “forward” scheme that removes progressively shorter nanotubes, and a “reverse” scheme that removes progressively longer ones. AFM measurements show that DNA–SWCNT fractions with average lengths from 60–500 nm and with standard deviations of 30–40% have been achieved. Finally, we use optical absorption spectroscopy to show that PEG precipitation can also be used to improve purity levels of DNA–SWCNT dispersion.

## RESULTS AND DISCUSSION

**Clustering of DNA–SWCNT under Crowded Conditions.** To observe PEG-induced clustering *in situ*, we start with DNA–SWCNTs purified and length-sorted by SEC.<sup>23</sup> We then take advantage of SWCNT band gap fluorescence,<sup>46</sup> acquiring fluorescence microscopy images of the DNA–SWCNT suspension before and after the addition of PEG. We begin with 20  $\mu\text{g}/\text{mL}$  of  $\sim 370$  nm

long DNA–SWCNT, and add increasing amount of 6 kDa PEG. As shown in Figure 1B, the initial addition of 1% mass fraction of PEG does not produce clustering; at 2%, rodlike microclusters 1–10  $\mu\text{m}$  long form; at 3%, the rodlike clusters further aggregate, forming loose assemblies, which can be pelleted by gentle centrifugation. When the pellet is redispersed in PEG-free buffer, no clusters are observed, suggesting cluster formation is reversible. To further illustrate reversibility, we measured excitonic energy transfer (EET) between nanotubes at each stage (Supporting Information, Figure S1). EET occurs when energy absorbed by one nanotube is transferred to, and possibly emitted by, a nearby nanotube.<sup>47</sup> Thus, EET serves as an indicator of nanotube proximity. In the presence of 7% PEG, SWCNTs indeed exhibit EET (see Supporting Information, Figure S1), although to a lower extent than completely bundled nanotubes,<sup>47</sup> presumably due to DNA and water layers separating individual SWCNTs in clusters. Redispersing SWCNT clusters in PEG-free buffer eliminates EET, demonstrating complete redispersion of the SWCNTs.

From counts of visible clusters, we estimate that at 2% PEG each cluster (1–10  $\mu\text{m}$  long) consists of between 1000 and 10 000 SWCNTs. To study cluster structure, we examine cluster fluorescence under polarized light (Figure 1C). For any chosen cluster, as the polarizer is rotated from parallel to perpendicular orientation with respect to the cluster axis, the brightness of the cluster decreases below a detectable limit. For example, the circled cluster vanishes in the upper left panel of Figure 1C. Fluorescence anisotropy in SWCNTs is caused by the axial polarization of the  $E_{11}$  van Hove transitions of semiconducting tubes.<sup>48</sup> The high anisotropy observed in fluorescence of these clusters indicates a high degree of SWCNT alignment along the cluster axis. Note that in our configuration both excitation and emission photons pass through the polarizer, thus the brightness of DNA–SWCNT must vary as  $\cos^4 \theta$ , where  $\theta$  is the angle between polarizer orientation and the nanotube axis. The brightness of a single nanotube would decay by 50% when  $\theta = 33^\circ$ . These  $33^\circ$  angles are indicated by dotted lines in Figure 1C. Qualitatively, we observe this decay behavior for the rodlike clusters.

**Length Dependence of SWCNT Clustering.** To examine length dependence of SWCNT clustering, we prepared length-fractionated DNA–SWCNT samples with SEC.<sup>23</sup> The fractions tested were  $370 \pm 100$ ,  $220 \pm 50$ , and  $150 \pm 30$  nm. The concentration of PEG was increased sequentially in 0.5% increments, and clustered DNA–SWCNTs were removed by centrifugation. The concentration of remaining nanotubes, which we define here as the nanotube solubility  $S$  at a given PEG concentration  $C$ , was quantified using SWCNT optical absorbance (see Methods for detail). The result is given in Figure 2, which shows that shorter nanotubes, 220 and 150 nm,

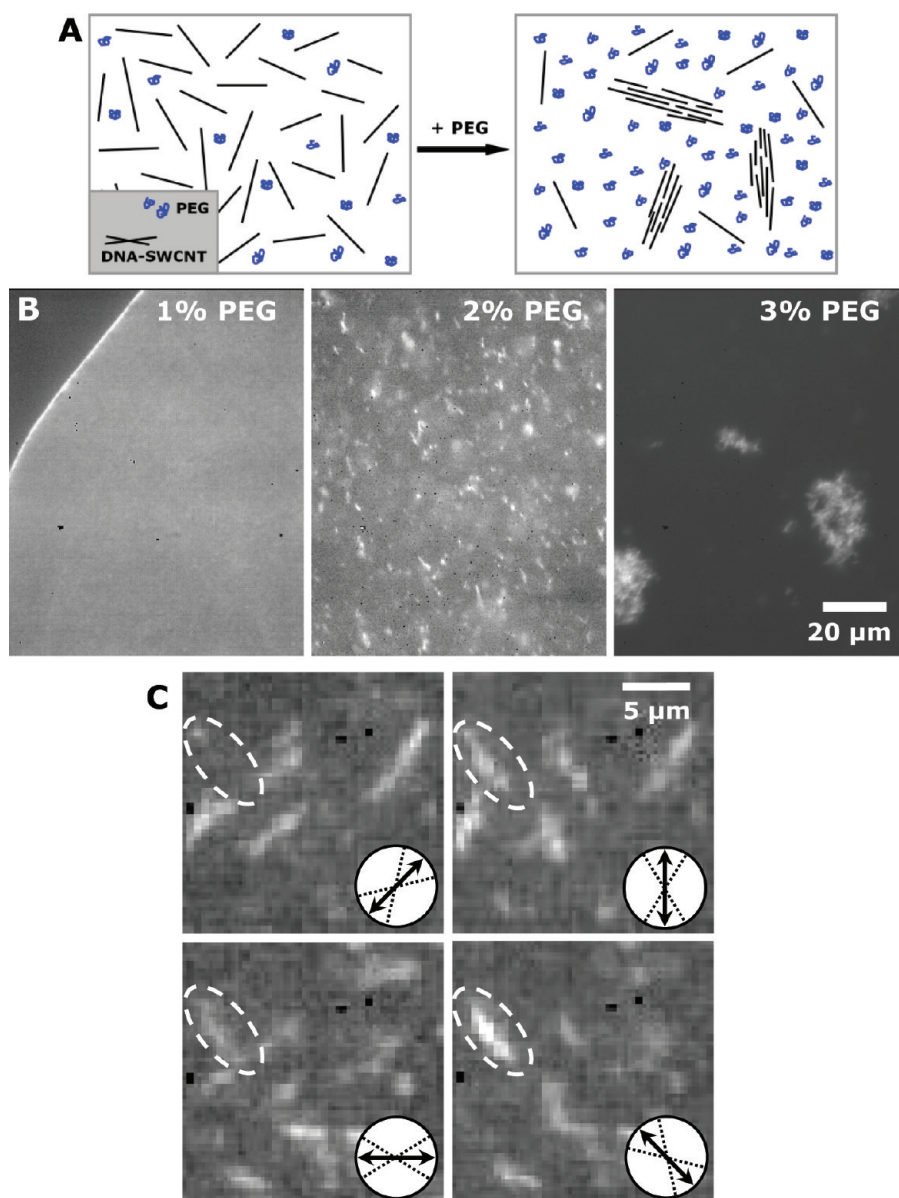


**Figure 1.** Cluster formation of DNA–SWCNT under crowded conditions. (A) Schematics showing DNA–SWCNTs are expected to form clusters in the presence of PEG due to attractive depletion forces. (B) Fluorescence microscopy images showing that DNA–SWCNTs remain well-dispersed in 1% PEG but form rodlike clusters at 2%. These clusters further aggregate into loose assemblies at 3% PEG. (C) Fluorescence microscopy images from the same group of microclusters viewed with four different polarizer orientations. A cluster is only visible when the orientation of the polarizer is close to the cluster axis, indicating that DNA–SWCNTs are aligned along that direction.

require  $1.2\times$  and  $1.4\times$  more PEG, respectively, to achieve the same solubility as 370 nm DNA–SWCNT. Also shown in Figure 2 is that each data set from a given length fraction can be modeled by the following general expression:  $\ln(S) = \ln(S_0) - \beta C$ , where  $S_0$  and  $\beta$  are fitting parameters given in Supporting Information, Table S1. Similar behavior has been observed in PEG precipitation of proteins,<sup>49</sup> which has been interpreted as evidence for depletion-induced clustering.<sup>49</sup>

**Schemes for Length Fractionation.** The length-dependence and reversibility of crowding-induced cluster formation suggest that it could be used to fractionate DNA–SWCNT raw material by selective precipitation.

We implemented two schemes, “forward sequential precipitation” and “reverse sequential precipitation”, as outlined in Figure 3.

In the forward sequential precipitation scheme (Figure 3A), a small amount of PEG (*e.g.*, 1.4%) is initially added to a DNA–SWCNT dispersion. Incubation followed by centrifugation (see Methods for details) produces a pellet containing the longest DNA–SWCNT. The supernatant is removed and the PEG concentration is increased (*e.g.*, by 0.4%), while the pellet is redispersed in PEG-free buffer. Incubation of the supernatant at higher PEG concentration followed by centrifugation produces a second pellet, of shorter

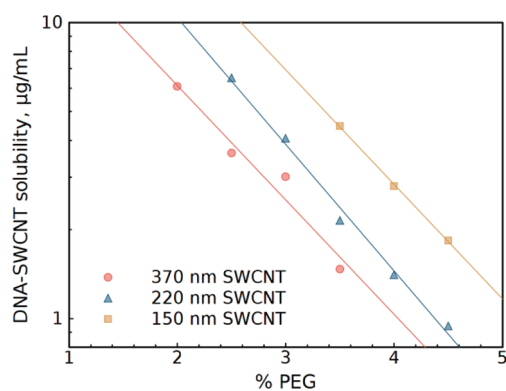


**Figure 2.** The measured solubility of DNA–SWCNT as a function of PEG concentration and DNA–SWCNT length.

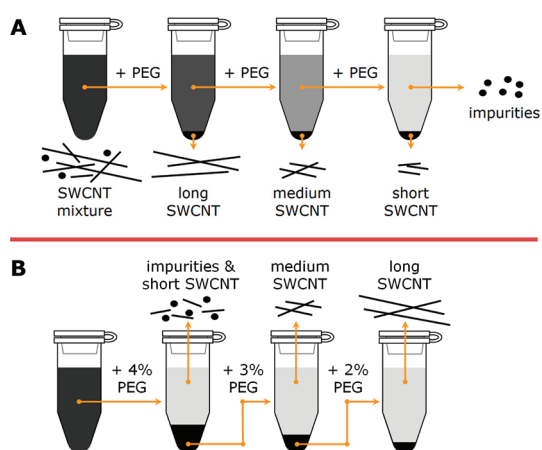


**Figure 3.** Two schemes for selective precipitation of DNA–SWCNT with PEG. (A) Forward sequential precipitation isolates progressively shorter DNA–SWCNT using stepwise increases in PEG concentration. (B) Reverse sequential precipitation isolates progressively longer DNA–SWCNT using stepwise decreases in PEG concentration: a pellet obtained from precipitation at a higher PEG concentration is redispersed in a lower PEG concentration to produce a soluble supernatant and a smaller pellet. The latter is used for the next round of solubilization and precipitation.

DNA–SWCNT, etc. In this scheme, progressively shorter DNA–SWCNTs are precipitated from the mixture until only impurities remain in the supernatant. Similar methods have been used for protein purification by PEG precipitation<sup>40,50</sup> and for the length fractionation of double stranded DNA.<sup>41</sup>

Reverse sequential precipitation (Figure 3B) begins with precipitation of all SWCNT lengths at a high PEG concentration (e.g., 4%). In this case the resulting pellet would be redispersed in 3% PEG solution; after incubation and centrifugation, a new pellet is produced containing medium and long DNA–SWCNTs, while short nanotubes remain in the supernatant. This pellet is once again redispersed, and the process continues until the desired fraction of long nanotubes is obtained in the supernatant. The final precipitate is discarded,

since it contains SWCNTs which aggregated during the process. This method isolates fractions of progressively longer SWCNTs from the mixture, and thus is optimal for obtaining pure fractions of long SWCNTs. Below, we show that these schemes are realized in practice.

**Determination of Length Distribution: Forward Sequential Precipitation.** To test the limit of length resolution attainable with this method, we performed a forward sequential precipitation experiment with small stepwise increases in PEG mass fraction: 1.4 → 1.9 → 2.3 → 2.8 → 3.2 → 3.7 → 4.1 → 4.6 → 5.0 → 5.4 → 5.9 → 6.5 → 7.2 → 8.5 %. Figure 4 gives AFM data showing that long nanotubes are preferentially precipitated first, followed by progressively shorter tubes. From the AFM images and histograms it can be readily seen that long fractions have broader length distribution. This is because the raw material contains a higher concentration of medium nanotubes than long nanotubes. From Figure 2 it is apparent that when sufficient PEG is added to precipitate long nanotubes, medium nanotubes will also be precipitated if they are present at a high enough concentration.

**Determination of Length Distribution: Reverse Sequential Precipitation.** As we have shown above, forward sequential precipitation (Figure 3A) yields higher length uniformity for short nanotube fractions, since long nanotubes are removed first. On the other hand, reverse sequential precipitation (Figure 3B) should yield long fractions of improved length uniformity, since short SWCNTs are preferentially removed first. Here, we progressively reduce the PEG concentration as follows: 4 → 3 → 2.5 → 2.1 → 1.7 → 1.3 wt %. The supernatants are retained for analysis. AFM measurements of the 2.1% and 1.3% supernatants show DNA–SWCNTs of length  $280 \pm 110$  nm (Figure 5 A,B), and  $490 \pm 190$  nm (Figure 5C,D), respectively. The histogram for each fraction also compares that from a “forward” sequential precipitation fraction, with the closest average length (Figure 5A,C).

As shown in Figure 5A, the 280 nm long fractions have similar length distributions. On the other hand, the long 490 nm fraction from reverse sequential precipitation shows a tighter length distribution (standard deviation of 190 vs 290 nm, Figure 5C). The difference is also visible qualitatively when comparing images of the long fractions in Figures 4A and 5D. The number of particulate and small nanotubes is lower in the reverse sequential precipitation scheme. The number of bundled nanotubes visible in the AFM images is also lower, likely because the sample examined is from the supernatant and bundles have been removed by precipitation and centrifugation. Thus, if long nanotube fractions with narrow length distributions are desired, reverse sequential precipitation should be used.

**Impurity Removal by PEG-Induced Clustering.** We found that impurity levels of DNA–SWCNT dispersion can be improved by PEG precipitation, as evidenced by the

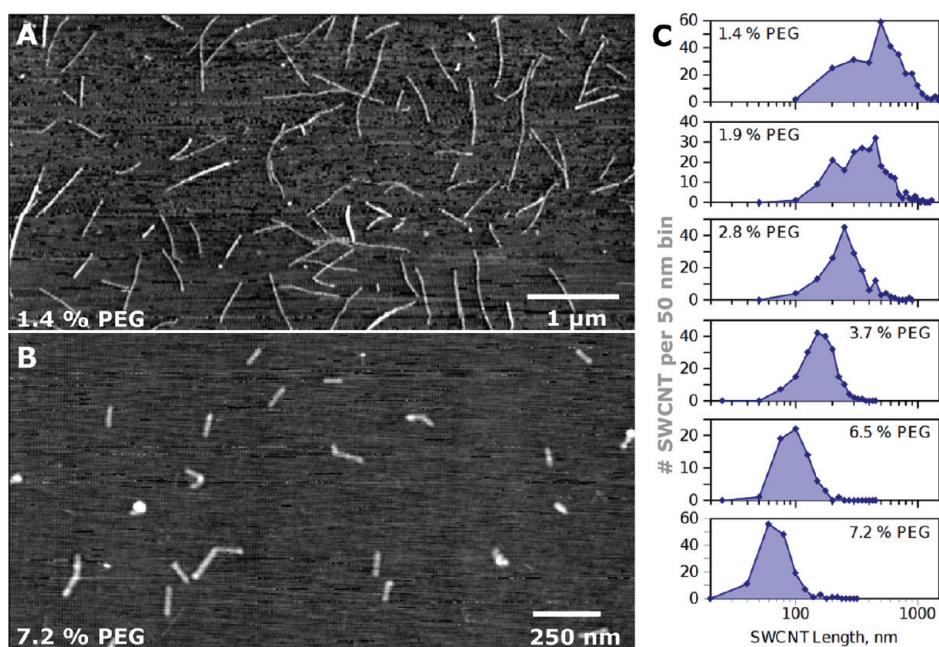


Figure 4. AFM images and length distribution of DNA–SWCNT from forward sequential precipitation.

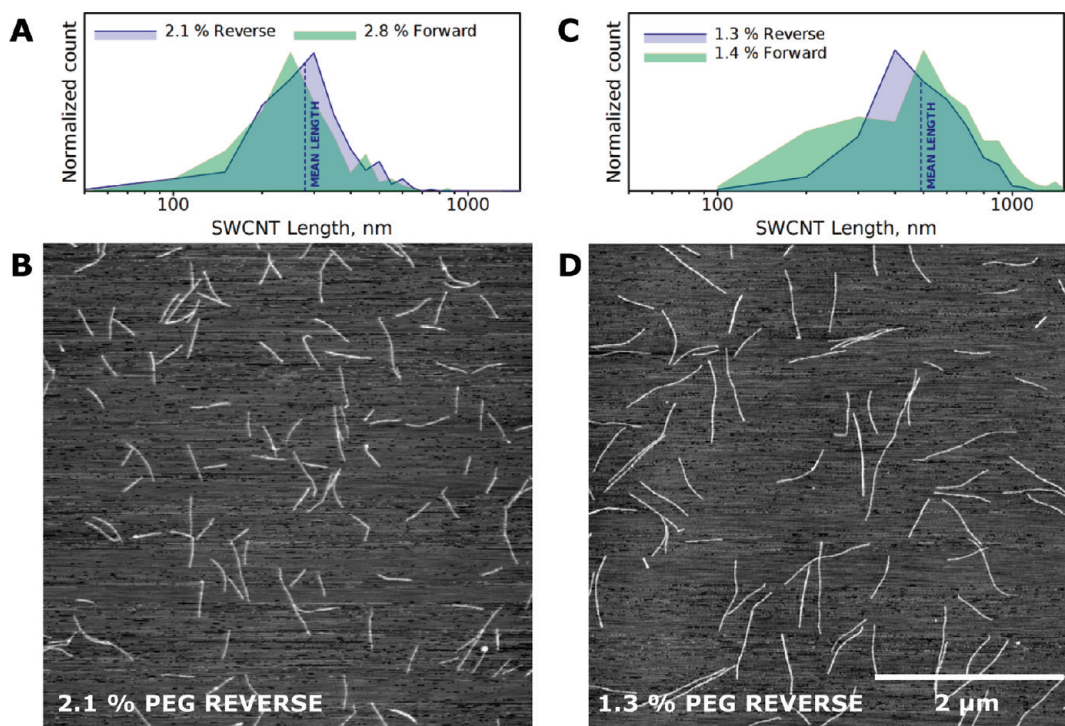


Figure 5. Length distributions of fractionated DNA–SWCNTs obtained by reverse sequential precipitation. In this scheme, progressive removal of short SWCNTs produces similar quality medium length fractions (left panels) but more uniform long SWCNT fractions (right panels).

optical absorption spectra of length-fractionated tubes. Electronic transitions in pure nanotubes produce prominent optical absorption peaks, dubbed E11, E22, and E33 for semiconducting nanotubes, and M11, M22 for metallic ones, with minimum reported baselines on the order of 2% of peak heights.<sup>7,8,51</sup> The presence of impurities results in an increase in baseline

by contributing a monotonic-decay component to the spectrum. For these reasons, optical absorption spectroscopy can be employed to quantify impurities in nanotube dispersions.

Forward sequential PEG precipitation improves the purity of SWCNT dispersions. Figure 6 compares the absorption spectra of the raw material, redispersed

precipitate, and two supernatants. Here, the precipitate was obtained after addition of 1.9% PEG in the same experiment shown in Figure 4, while the two supernatants were leftovers after precipitation with 5.9% PEG and 8.5% PEG in the same experiment. It is evident from Figure 6 that the baseline is lower in the precipitated SWCNTs and higher in the supernatants. Whereas there are still nanotubes present after 5.9% precipitation, no nanotubes appear to be soluble in 8.6% PEG. Optical absorption spectra for additional samples from the forward precipitation series are given in Supporting Information, Figure S2. Pellets up to 3.7% PEG,  $160 \pm 50$  nm, show baseline improvement over the starting material; shorter SWCNTs have gradually higher baselines. Similar absorbance spectra were obtained for SWCNT fractions from the reverse sequential precipitation experiment. Absorption baseline increase for short SWCNTs has been observed for the SEC length-fractionation technique, and has been interpreted as the consequence of small graphitic and fullerene impurities.<sup>23</sup>

**Influence of Dispersant: DNA Oligomers vs Yeast RNA.** We also tested baker's yeast RNA as an alternative to the more expensive DNA oligomers for SWCNT dispersion. RNA–SWCNT raw material shows similar absorbance spectra and fluorescent brightness, especially after surfactant displacement of the DNA/RNA<sup>52</sup> (Supporting Information, Figure S3A,B). PEG precipitation using the forward sequential scheme (Figure 3A) yields improved spectral characteristics (see Figure S3C) similar to the improvement for DNA–SWCNT (Figure S2). AFM characterization of length distribution for one sample shows that the average length of precipitated CNTs is comparable to DNA–SWCNT (at ~3% PEG) but the standard deviation is larger (Figure S3D,E). The reverse sequential scheme (Figure 3B) does not work with RNA–SWCNT: after two precipitation cycles, all SWCNTs precipitate, even with RNA added to keep a constant unbound RNA concentration. This result suggests RNA binding to SWCNTs is weaker than the (GT)<sub>20</sub>. Nevertheless, RNA–SWCNT purification by forward sequential precipitation could be useful if cost is an issue.

**Influence of PEG Molecular Weight.** We found that there is an optimal range of PEG molar mass for DNA–SWCNT precipitation. We measured the total fraction of nanotube raw material precipitated during forward sequential precipitation (defined as yield) for several PEGs with different molecular weights (MW). These results are shown in Supporting Information, Figure S4. We observed different behaviors for different PEG concentrations. At low PEG concentrations, yield decreases with reducing PEG molecular weight in the following order: 12 kDa > 6 kDa > 1.5 kDa (with 600 Da PEG producing no precipitation), but does not show much difference for MW > 12 kDa. A similar dependence has been observed for both rodlike viruses<sup>39</sup> and globular proteins.<sup>49</sup> It has been proposed for

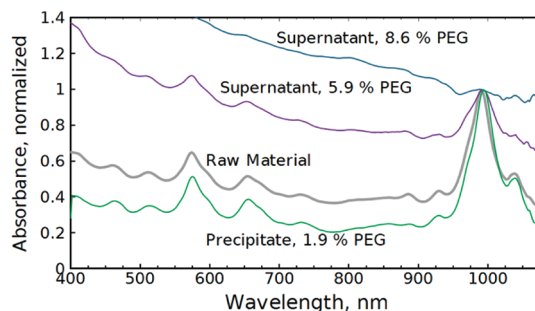


**Figure 6.** Optical absorption spectra (normalized at 990 nm) of different fractions obtained by the forward precipitation experiment shown in Figure 4.

viruses (and may be true for DNA–SWCNT as well) that clusters contain large interstitial spaces due to electrostatic repulsion and small PEG molecules are not effectively excluded, thus losing their crowding power.<sup>39</sup> At high PEG concentrations, PEG with MW > 12 kDa progressively loses precipitating power. At the extreme, addition of more than 2% PEG of 300 kDa does not produce further DNA–SWCNT precipitation, and a maximum yield of only 0.05 is obtained. Considering also the higher viscosity of high MW PEG solutions, we concluded that 6–12 kDa PEGs are optimal for length fractionation.

## CONCLUDING REMARKS

We employed PEG-induced clustering of DNA–SWCNT for length fractionation. Although the length uniformity is less than that attainable with SEC, the PEG precipitation method is far more facile and scalable since it does not require elaborate equipment. It is our hope that this method can be adapted for different purification needs—whether to SWCNT systems or perhaps to other nanoparticles. The following is a summary of considerations for adaptation.

1. Although many precipitation steps were used in this report, even one-step precipitation yields noticeable improvements in both length uniformity and purity, and could be sufficient for some applications.
2. The optimal PEG molecular weight for purification is 6–12 kDa.
3. If short nanotube fractions with narrow length distribution are desired, “forward sequential precipitation” should be employed; for long nanotube fractions “reverse sequential precipitation” is preferable.

It should be noted that the length fractionation mechanism we presented in this work relies on a purely entropic effect of the crowding agent. However, recent theoretical analyses suggest that enthalpic interactions between a colloid and a crowding agent may dramatically alter the colloid solubility, to the degree that the enthalpic effect completely negates attractive entropic forces.<sup>37,53</sup> Such “enthalpy–entropy

compensation" suggests that by employing chirality-dependent polymer/SWCNT interactions between DNA–SWCNT and a crowding agent, it may be possible

to achieve chirality fractionation of SWCNTs. Studies in this direction are underway in our laboratory and will be reported elsewhere in the future.

## METHODS

Certain commercial equipment, instruments, or materials are identified in this paper in order to specify the experimental procedure adequately. Such identification is not intended to imply recommendation or endorsement by the National Institute of Standards and Technology, nor is it intended to imply that the materials or equipment identified are necessarily the best available for the purpose. Unless noted otherwise, all reagents were obtained from standard sources. The symbol " $\pm$ " is used here to indicate an interval of one standard deviation, unless otherwise noted.

**Dispersion of SWCNTs.** SWCNTs (grade S-P95-02-Dry, batch Du1-A001 CoMoCat) are purchased from Southwest Nanotechnologies (Norman, OK), DNA oligomers from IDT-DNA (Coralville, IA), and baker's yeast RNA (R6750) from Sigma-Aldrich Co. (St. Louis, MO). SWCNTs were suspended in DI water at a concentration of 1 mg/mL by sonicating for 5 min at 6 W with a 3 mm diameter probe sonicator. This stock solution was used to create 1 mg pellets of SWCNT material for dispersion. To the 1 mg pellet were added 120  $\mu$ L of 10 mg/mL (GT)<sub>20</sub> oligomer in 2x SSC buffer (30 mmol/L sodium citrate, 300 mmol/L sodium chloride) and 880  $\mu$ L of additional 2x SSC buffer. As a substitute of DNA, 150  $\mu$ L of baker's yeast RNA at 10 mg/mL may be used (see main text), but RNA concentration must be verified by UV–vis spectroscopy. The DNA (or RNA)/SWCNT mixture was sonicated for 60 min at 6 W with a 3 mm probe sonicator in a 1.5 mL microcentrifuge tube, with the probe 5 mm above the tube bottom. The resulting suspension was centrifuged at 18 °C and 17 000 *g* in 100  $\mu$ L aliquots for 90 min. The supernatant was collected and used without further processing.

**Forward Sequential Precipitation.** Since nanotube solubility decreases by 1 order of magnitude for a PEG concentration increase of 2.5% (Figure 2), this factor can be used to adjust PEG concentration for working with SWCNT raw material of different concentrations. The dry PEG material was protected from moisture; only freshly purchased material was used, since older material gave unpredictable variations in results. In a typical run, a DNA–SWCNT or RNA–SWCNT dispersion was diluted to a final concentration of 80  $\mu$ g/mL SWCNTs (using the published value of 13  $\mu$ g/mL for OD = 1 at 990 nm for (6,5) enriched CoMoCAT<sup>54</sup>). A final concentration of 500 mmol/L NaCl was then added, and 50% stock PEG solution was added to the desired final concentration for the first precipitation step. The SWCNT/PEG mixture was incubated overnight at 4 °C for PEG concentrations <4%, or two days at 4 °C for PEG concentrations >4%. Incubation at higher temperature was found to require longer time and higher PEG concentration to achieve similar levels of precipitation. After incubation, the mixture was centrifuged at 18 °C and 8000 *g* for 10 min. If the pellet was not tight, the centrifuge tube was rotated 180° and centrifuged again. The supernatant was removed and more PEG was added to the supernatant to increase the concentration for the next precipitation step. The pellet was redispersed, by pipetting several times, in 100 mmol/L NaCl, for further analysis. An additional amount of DNA can be added to a final concentration of 100  $\mu$ g/mL for improved stability of purified DNA–SWCNT for long-term storage.

**Reverse Sequential Precipitation.** The basic precipitation procedures in this scheme are identical to the forward precipitation scheme described above. Since in this scheme the supernatant contains the desired fractionated SWCNTs, the free PEG may be removed from the supernatant, if desired, by PEG precipitation at a higher concentration, or by dialysis. The pellet is resuspended with a lower PEG concentration for the next fractionation step. A final concentration of 100  $\mu$ g/mL (GT)<sub>20</sub> oligomer is added to maintain a concentration of free dispersant in the mixture (see below). These steps are repeated until the desired

fraction of nanotubes is isolated in the supernatant (for example, the pellet from 2% precipitation is resuspended in 1.5% 6 kDa PEG; after pelleting at 1.5% the supernatant would have long, ~500 nm SWCNTs).

During forward sequential precipitation, unbound DNA left over from the dispersion process is constantly present in the supernatant. On the other hand, during reverse sequential precipitation, pelleting and redispersion removes unbound DNA from the solution. We found that pellets formed in the absence of free DNA cannot be redispersed. A constant concentration of unbound DNA must be maintained during reverse sequential precipitation (here 100  $\mu$ g/mL) to avoid irreversible aggregation of SWCNTs.

**Polarized Fluorescence Microscopy.** Microscopy was carried out on an Olympus IX71 inverted microscope with a standard 100 W mercury light source and a 60x water immersion objective (IR-enhanced Olympus UPlanSAppo). A filter cube composed of a 570 nm, 10 nm bandpass excitation filter (Andover Co., cat no. 570FS10-25) and a 950 nm long-pass emission filter (Chroma Inc., cat no. 950LP 66921) was used. A PI Acton model 7531 camera (Princeton Instruments Inc.) was used for image acquisition. Finally, an IR polarizer (Edmund Optics NT47-327, contrast 10<sup>3</sup> at 575 nm and 10<sup>6</sup> at 990 nm, was placed between the filter wheel and the objective and rotated manually.

**Atomic Force Microscopy.** Freshly cleaved mica was used for sample deposition. The DNA–SWCNT sample was diluted to a final concentration of ~1  $\mu$ g/mL into 15 mmol/L KCl. Since KCl neutralizes the charge on Muscovite mica,<sup>55</sup> deposition was rapid and a sufficient number of SWCNTs was observed after 2–15 min of incubation. An MFP3D AFM (Asylum Research, Santa Barbara, CA) was used for observations. Typically, 200 to 500 SWCNTs were measured for each histogram.

**Optical Absorbance and Fluorescence Measurements.** Samples were diluted to OD  $\approx$  1 at 990 nm with DI water and measured in a 100  $\mu$ L microcuvette against DI water as baseline on a Biomet 6 (ThermoFisher Scientific) spectrophotometer. Fluorescence measurements were made using a Horiba Jobin Yvon Nanolog-3 spectrofluorometer with a liquid nitrogen-cooled Symphony InGaAs detector. The sample was measured in a 2  $\times$  10 mm quartz cuvette at an OD  $\approx$  0.2 at 990 nm. A 645 nm long-pass filter was placed after the sample to eliminate the second harmonic signal due to strong scattering by SWCNT clusters. The light source was a 450 W xenon lamp. The emission spectra were corrected for the wavelength dependence of the excitation intensity and the wavelength dependent efficiency of the detector train. Replacement of DNA by sodium deoxycholate (SDC) was achieved by simply adding 10% SDC to the DNA–SWCNT sample to a final mass fraction of 1%.

**Supporting Information Available:** SWCNT solubility data in the presence of PEG, fluorescence measurements of EET in SWCNT clusters, data for RNA–SWCNT sequential precipitation, optical absorption spectra of purified SWCNTs, and yield as a function of PEG molecular weight for forward sequential precipitation. This material is available free of charge via the Internet at <http://pubs.acs.org>.

**Acknowledgment.** The authors would like to thank Dr. Jack Douglas for invaluable discussions on molecular crowding, as well as Dr. Xiaomin Tu for help and support. Finally, many thanks to Dr. Denis Pristinski for help with optics engineering.

## REFERENCES AND NOTES

- Hersam, M. Progress Towards Monodisperse Single-Walled Carbon Nanotubes. *Nat. Nanotechnol.* **2008**, *3*, 387–394.
- Tu, X.; Zheng, M. A DNA-Based Approach to the Carbon Nanotube Sorting Problem. *Nano Res.* **2008**, *1*, 185–194.

3. Liu, J.; Hersam, M. C. Recent Developments in Carbon Nanotube Sorting and Selective Growth. *MRS Bull.* **2010**, *35*, 315–322.
4. Zheng, M.; Semke, E. D. Enrichment of Single Chirality Carbon Nanotubes. *J. Am. Chem. Soc.* **2007**, *129*, 6084–6085.
5. Ju, S. Y.; Doll, J.; Sharma, I.; Papadimitrakopoulos, F. Selection of Carbon Nanotubes with Specific Chiralities Using Helical Assemblies of Flavin Mononucleotide. *Nature Nanotechnol.* **2008**, *3*, 356–362.
6. Ghosh, S.; Bachilo, S. M.; Weisman, R. B. Advanced Sorting of Single-Walled Carbon Nanotubes by Nonlinear Density-Gradient Ultracentrifugation. *Nat. Nanotechnol.* **2010**, *5*, 443–450.
7. Tu, X.; Manohar, S.; Jagota, A.; Zheng, M. DNA Sequence Motifs for Structure-Specific Recognition and Separation of Carbon Nanotubes. *Nature* **2009**, *460*, 250–253.
8. Tu, X.; Hight-Walker, A. R.; Khripin, C. Y.; Zheng, M. Evolution of DNA Sequences Towards Recognition of Metallic Armchair Carbon Nanotubes. *J. Am. Chem. Soc.* **2011**, *133*, 12998–13001.
9. Liu, H.; Nishide, D.; Tanaka, T.; Kataura, H. Large-Scale Single-Chirality Separation of Single-Wall Carbon Nanotubes by Simple Gel Chromatography. *Nat. Commun.* **2011**, *2*, 309.
10. Avouris, P.; Chen, Z.; Perebeinos, V. Carbon-Based Electronics. *Nat. Nanotechnol.* **2007**, *2*, 605–615.
11. Fagan, J. A.; Simpson, J. R.; Bauer, B. J.; Lacerda, S. H. D. P.; Becker, M. L.; Chun, J.; Migler, K. B.; Walker, A. R. H.; Hobbie, E. K. Length-Dependent Optical Effects in Single-Wall Carbon Nanotubes. *J. Am. Chem. Soc.* **2007**, *129*, 10607–10612.
12. Miyauchi, Y.; Matsuda, K.; Yamamoto, Y.; Nakashima, N.; Kanemitsu, Y. Length-Dependent Photoluminescence Lifetimes in Single-Walled Carbon Nanotubes. *J. Phys. Chem. C* **2010**, *114*, 12905–12908.
13. Hertel, T.; Himmelein, S.; Ackermann, T.; Stich, D.; Crochet, J. Diffusion Limited Photoluminescence Quantum Yields in 1-D Semiconductors: Single-Wall Carbon Nanotubes. *ACS Nano* **2011**, *4*, 7161–7168.
14. Robinson, J. T.; Welsher, K.; Tabakman, S. M.; Sherlock, S. P.; Wang, H.; Luong, R.; Dai, H. High Performance *in Vivo* near-Ir (>1 M) Imaging and Photothermal Cancer Therapy with Carbon Nanotubes. *Nano Res.* **2010**, DOI 10.1007/s12274-010-0045-1.
15. Becker, M. L.; Fagan, J. A.; Gallant, N. D.; Bauer, B. J.; Bajpai, V.; Hobbie, E. K.; Lacerda, S. H.; Migler, K. B.; Jakupciak, J. P. Length Dependent Uptake of DNA-Wrapped Single Walled Carbon Nanotubes. *Adv. Mater.* **2007**, *19*, 939–945.
16. Feazell, R. P.; Nakayama-Ratchford, N.; Dai, H.; Lippard, S. J. Soluble Single-Walled Carbon Nanotubes as Longboat Delivery Systems for Platinum (IV) Anticancer Drug Design. *J. Am. Chem. Soc.* **2007**, *129*, 8438–8439.
17. Liu, Z.; Chen, K.; Davis, C.; Sherlock, S.; Cao, Q.; Chen, X.; Dai, H. Drug Delivery with Carbon Nanotubes for *in Vivo* Cancer Treatment. *Cancer Res.* **2008**, *68*, 6652.
18. Cai, D.; Mataraza, J. M.; Qin, Z. H.; Huang, Z.; Huang, J.; Chiles, T. C.; Carnahan, D.; Kempa, K.; Ren, Z. Highly Efficient Molecular Delivery into Mammalian Cells Using Carbon Nanotube Sparring. *Nat. Methods* **2005**, *2*, 449–454.
19. Liu, Z.; Tabakman, S.; Welsher, K.; Dai, H. Carbon Nanotubes in Biology and Medicine: *In Vitro* and *in Vivo* Detection, Imaging and Drug Delivery. *Nano Res.* **2009**, *2*, 85–120.
20. Duesberg, G. S.; Muster, J.; Krstic, V.; Burghard, M.; Roth, S. Chromatographic Size Separation of Single-Wall Carbon Nanotubes. *Appl. Phys. A: Mater. Sci. Process.* **1998**, *67*, 117–119.
21. Duesberg, G. S.; Blau, W.; Byrne, H. J.; Muster, J.; Burghard, M.; Roth, S. Chromatography of Carbon Nanotubes. *Synth. Met.* **1999**, *103*, 2484–2485.
22. Farkas, E.; Elizabeth Anderson, M.; Chen, Z.; Rinzler, A. G. Length Sorting Cut Single Wall Carbon Nanotubes by High Performance Liquid Chromatography. *Chem. Phys. Lett.* **2002**, *363*, 111–116.
23. Huang, X.; Mclean, R. S.; Zheng, M. High-Resolution Length Sorting and Purification of DNA-Wrapped Carbon Nanotubes by Size-Exclusion Chromatography. *Anal. Chem.* **2005**, *77*, 6225–6228.
24. Bauer, B. J.; Fagan, J. A.; Hobbie, E. K.; Chun, J.; Bajpai, V. Chromatographic Fractionation of SWNT/DNA Dispersions with on-Line Multi-angle Light Scattering. *J. Phys. Chem. C* **2008**, *112*, 1842–1850.
25. Fagan, J. A.; Becker, M. L.; Chun, J.; Hobbie, E. K. Length Fractionation of Carbon Nanotubes Using Centrifugation. *Adv. Mater.* **2008**, *20*, 1609–1613.
26. Sun, X.; Zaric, S.; Darancioglu, D.; Welsher, K.; Lu, Y.; Li, X.; Dai, H. Optical Properties of Ultrashort Semiconducting Single-Walled Carbon Nanotube Capsules Down to Sub-10 Nm. *J. Am. Chem. Soc.* **2008**, *130*, 6551–6555.
27. Chen, B.; Selegue, J. Separation and Characterization of Single-Walled and Multiwalled Carbon Nanotubes by Using Flow Field-Flow Fractionation. *Anal. Chem.* **2002**, *74*, 4774–4780.
28. Chun, J.; Fagan, J. A.; Hobbie, E. K.; Bauer, B. J. Size Separation of Single-Wall Carbon Nanotubes by Flow-Field Flow Fractionation. *Anal. Chem.* **2008**, *80*, 2514–2523.
29. Ohmori, S.; Saito, T.; Shukla, B.; Yumura, M.; Iijima, S. Fractionation of Single Wall Carbon Nanotubes by Length Using Cross Flow Filtration Method. *ACS Nano* **2010**, *4*, 3606–3610.
30. Chou, S. G.; Son, H.; Kong, J.; Jorio, A.; Saito, R.; Zheng, M.; Dresselhaus, G.; Dresselhaus, M. S. Length Characterization of DNA-Wrapped Carbon Nanotubes Using Raman Spectroscopy. *Appl. Phys. Lett.* **2007**, *90*, 131109.
31. Medalia, O.; Weber, I.; Frangakis, A. S.; Nicastrò, D.; Gerisch, G.; Baumeister, W. Macromolecular Architecture in Eukaryotic Cells Visualized by Cryoelectron Tomography. *Science* **2002**, *298*, 1209.
32. Miyoshi, D.; Sugimoto, N. Molecular Crowding Effects on Structure and Stability of DNA. *Biochimie* **2008**, *90*, 1040–1051.
33. Minton, A. P. Implications of Macromolecular Crowding for Protein Assembly. *Curr. Opin. Struct. Biol.* **2000**, *10*, 34–39.
34. Asakura, S.; Oosawa, F. On Interaction between Two Bodies Immersed in a Solution of Macromolecules. *J. Chem. Phys.* **1954**, *22*, 1255–1256.
35. Tuinier, R.; Rieger, J.; De Kruijff, C. G. Depletion-Induced Phase Separation in Colloid-Polymer Mixtures. *Adv. Colloid Interfac.* **2003**, *103*, 1–31.
36. Stradner, A.; Sedgwick, H.; Cardinaux, F.; Poon, W. C. K.; Egelhaaf, S. U.; Schurtenberger, P. Equilibrium Cluster Formation in Concentrated Protein Solutions and Colloids. *Nature* **2004**, *432*, 492–495.
37. Douglas, J. F.; Dudowicz, J.; Freed, K. F. Crowding Induced Self-Assembly and Enthalpy–Entropy Compensation. *Phys. Rev. Lett.* **2009**, *103*, 135701.
38. Buitenhuis, J.; Donselaar, L. N.; Buining, P. A.; Stroobants, A.; Lekkerkerker, H. N. W. Phase Separation of Mixtures of Colloidal Boehmite Rods and Flexible Polymer. *J. Colloid Interface Sci.* **1995**, *175*, 46–56.
39. Adams, M.; Fraden, S. Phase Behavior of Mixtures of Rods (Tobacco Mosaic Virus) and Spheres (Polyethylene Oxide, Bovine Serum Albumin). *Biophys. J.* **1998**, *74*, 669–677.
40. Ingham, K. C. Protein Precipitation with Polyethylene Glycol. *Methods Enzymol.* **1984**, *104*, 351.
41. Lis, J. T.; Schleif, R. Size Fractionation of Double-Stranded DNA by Precipitation with Polyethylene Glycol. *Nucleic Acids Res.* **1975**, *2*, 383.
42. Zheng, M.; Jagota, A.; Strano, M. S.; Santos, A. P.; Barone, P.; Chou, S. G.; Diner, B. A.; Dresselhaus, M. S.; Mclean, R. S.; Onoa, G. B. Structure-Based Carbon Nanotube Sorting by Sequence-Dependent DNA Assembly. *Science* **2003**, *302*, 1545.
43. Zheng, M.; Jagota, A.; Semke, E.; Diner, B.; McLean, R.; Lustig, S.; Richardson, R.; Tassi, N. DNA-Assisted Dispersion and Separation of Carbon Nanotubes. *Nat. Mater.* **2003**, *2*, 338–342.
44. Khripin, C. Y.; Manohar, S.; Zheng, M.; Jagota, A. Measurement of Electrostatic Properties of DNA–Carbon Nanotube Hybrids by Capillary Electrophoresis. *J. Phys. Chem. C* **2009**, *113*, 13616–13621.
45. Zhao, K.; Mason, T. G. Directing Colloidal Self-Assembly through Roughness-Controlled Depletion Attractions. *Phys. Rev. Lett.* **2007**, *99*, 268301.

46. O'Connell, M. J.; Bachilo, S. M.; Huffman, C. B.; Moore, V. C.; Strano, M. S.; Haroz, E. H.; Rialon, K. L.; Boul, P. J.; Noon, W. H.; Kittrell, C. Band Gap Fluorescence from Individual Single-Walled Carbon Nanotubes. *Science* **2002**, *297*, 593.
47. Torrens, O. N.; Milkie, D. E.; Zheng, M.; Kikkawa, J. M. Photoluminescence from Intertube Carrier Migration in Single-Walled Carbon Nanotube Bundles. *Nano lett.* **2006**, *6*, 2864–2867.
48. Tsybouski, D. A.; Bachilo, S. M.; Weisman, R. B. Versatile Visualization of Individual Single-Walled Carbon Nanotubes with Near-Infrared Fluorescence Microscopy. *Nano lett.* **2005**, *5*, 975–979.
49. Atha, D. H.; Ingham, K. C. Mechanism of Precipitation of Proteins by Polyethylene Glycols. Analysis in Terms of Excluded Volume. *J. Biol. Chem.* **1981**, *256*, 12108.
50. Mahadevan, H.; Hall, C. K. Experimental Analysis of Protein Precipitation by Polyethylene Glycol and Comparison with Theory. *Fluid Phase Equilib.* **1992**, *78*, 297–321.
51. Nish, A.; Hwang, J. Y.; Doig, J.; Nicholas, R. J. Highly Selective Dispersion of Single-Walled Carbon Nanotubes Using Aromatic Polymers. *Nat. Nanotechnol.* **2007**, *2*, 640–646.
52. Roxbury, D.; Tu, X.; Zheng, M.; Jagota, A. Recognition Ability of DNA for Carbon Nanotubes Correlates with Their Binding Affinity. *Langmuir* **2011**, *27*, 8282–8293.
53. Rosen, J.; Kim, Y. C.; Mittal, J. Modest Protein-Crowder Attractive Interactions Can Counteract Enhancement of Protein Association by Intermolecular Excluded Volume Interactions. *J. Phys. Chem. B* **2011**, *115*, 2683–2689.
54. Zheng, M.; Diner, B. A. Solution Redox Chemistry of Carbon Nanotubes. *J. Am. Chem. Soc.* **2004**, *126*, 15490–15494.
55. Sides, P. J.; Faruqi, D.; Gellman, A. J. Dynamics of Charging of Muscovite Mica: Measurement and Modeling. *Langmuir* **2009**, *25*, 1475–1481.